Carbohydrate Polymers 321 (2023) 121261

Contents lists available at ScienceDirect

Carbohydrate Polymers

journal homepage: www.elsevier.com/locate/carbpol

A comparative analysis of pulp-derived nanocelluloses for 3D bioprinting facial cartilages

Thomas H. Jovic [a,b,*], Tamsin Nicholson [c], Hari Arora [c], Kim Nelson [d], Shareen H. Doak [c], Iain S. Whitaker [a,b]

[a] Reconstructive Surgery and Regenerative Medicine Research Centre, Institute of Life Sciences 1, Swansea University, SA2 8PP, UK
[b] Welsh Centre for Burns & Plastic Surgery, Morriston Hospital, Swansea SA6 6NL, UK
[c] Swansea University, Swansea SA2 8PP, UK
[d] GranBio, Sao Paolo, Brazil

ARTICLE INFO

Keywords:
Cartilage
Bioprinting
Nanocellulose
Alginate

ABSTRACT

Nanocelluloses have attracted significant interest in the field of bioprinting, with previous research outlining the value of nanocellulose fibrils and bacterial nanocelluloses for 3D bioprinting tissues such as cartilage. We have recently characterised three distinct structural formulations of pulp-derived nanocelluloses: fibrillar (NFC), crystalline (NCC) and blend (NCB), exhibiting variation in pore geometry and mechanical properties. In light of the characterisation of these three distinct entities, this study investigated whether these structural differences translated to differences in printability, chondrogenicity or biocompatibility for 3D bioprinting anatomical structures with human nasoseptal chondrocytes. Composite nanocellulose-alginate bioinks (75:25 v/v) of NFC, NCC and NCB were produced and tested for print resolution and fidelity. NFC offered superior print resolution whereas NCB demonstrated the best post-printing shape fidelity. Biologically, chondrogenicity was assessed using real time quantitative PCR, dimethylmethylene blue assays and histology. All biomaterials showed an increase in chondrogenic gene expression and extracellular matrix production over 21 days, but this was superior in the NCC bioink. Biocompatibility assessments revealed an increase in cell number and metabolism over 21 days in the NCC and NCB formulations. Nanocellulose augments printability and chondrogenicity of bioinks, of which the NCC and NCB formulations offer the best biological promise for bioprinting cartilage.

1. Introduction

The pursuit of clinically translatable bioinks demands a balance of both biological and mechanical characteristics. Specifically, characteristics of these biological inks ("bioinks") include adequate printability to confer shape fidelity and resolution in anatomical structures (Kyle et al., 2017) whilst possessing biological properties that support cell growth, adhesion and ideally cellular differentiation into the desired tissue type (Jessop et al., 2017; Kyle et al., 2017; Tarassoli et al., 2021). Achieving balance in these properties, known as the 'biofabrication window', is often fraught with conflict and has been a significant limitation in the optimisation of advanced biomaterials for three-dimensional (3D) bioprinting of human tissues (Chimene et al., 2016; Malda et al., 2013). Synthetic biomaterials, typically convey superiority in their mechanical and printability characteristics, with the additional advantages of being easily modifiable with regard to their strength and rheological properties (Jovic et al., 2019). A major drawback of synthetic materials is their limited bioactivity: a failure to mimic extracellular matrix (ECM) results in a poor affinity for cellular adhesion, growth, migration and differentiation (O'Brien, 2011). Of the biodegradable synthetic materials, the degradation process may result in the release of by-products presenting a risk of toxicity or immunogenicity when implanted into humans (Athanasiou et al., 1996; Taylor et al., 1994). Whereas the non-degradable synthetic materials, despite offering superior shape preservation, risk extrusion and impedance of de novo tissue formation which may limit their applicability in a clinical setting (Sarkar et al., 2017).

As such, there has been a progressive shift in focus towards refining natural materials for a variety of biomedical applications (Tarassoli

Abbreviations: NCC, Nanocellulose Crystals; NCB, Nanocellulose Blend; NFC, Nanocellulose Fibrils; DMMB, Dimethylmethylene Blue; AVAP, American Value Added Pulping.

* Corresponding author at: Reconstructive Surgery and Regenerative Medicine Research Centre, Institute of Life Sciences 1, Swansea University, SA2 8PP, UK.
E-mail address: t.h.jovic@swansea.ac.uk (T.H. Jovic).

https://doi.org/10.1016/j.carbpol.2023.121261
Received 23 June 2023; Received in revised form 28 July 2023; Accepted 3 August 2023
Available online 5 August 2023

et al., 2021). Plant-derived biomaterials offer the benefits of harnessing the structural microarchitecture of plants combined with their inherent ability to support cell growth (Gershlak et al., 2017; Jovic et al., 2019). Plant materials often offer biodegradability and mechanical stability in addition to their bioactivity making them strong candidates for 3D bioprinting (Yegappan et al., 2018). Their use as potential bioinks is strengthened by the potential for chemical modification and hydrogel formation. The abundance of these materials from natural and renewable sources has therefore garnered significant attention in the field of 3D bioprinting, with plant-derived biomaterials dominating 3D bioprinting research over the last decade (Tarassoli et al., 2021).

Alginate, derived from brown algae, is the most researched bioink in extrusion based 3D bioprinting (Lee & Mooney, 2012; Tarassoli et al., 2021) and has been a prevalent material in cartilage tissue engineering research efforts to date (Axpe & Oyen, 2016). Its affinity for cell encapsulation arises from its facile hydration into hydrogel suspensions and readiness to crosslink in the presence of divalent cations (Wee & Gombotz, 1998), making it an attractive material for cartilage tissue engineering purposes (Park et al., 2018).

In order to augment the printability, strength and bioactive potential of alginate bioinks for 3D bioprinting, previous research has examined the role of blending alginate with nanocelluloses for cartilage tissue engineering (Aarstad et al., 2017; Jessop et al., 2019; Markstedt et al., 2015; Martínez Ávila et al., 2015; Pääkko et al., 2007; Siqueira et al., 2019). The combination of the two materials in synergy was felt to offer superior printability characteristics including enhanced shear thinning, rapid crosslinking and shape fidelity with evidence of satisfactory cell survival in the material (Jessop et al., 2019; Markstedt et al., 2015; Müller et al., 2017). Furthermore, chondrocytes cultured in nanocellulose-alginate bioinks demonstrate proliferation and cartilage specific gene expression (Type 2 Collagen) over time indicating an inherent chondrogenicity of this material combination (Müller et al., 2017).

Nanocellulose has attracted significant attention in the field of 3D bioprinting owing to its excellent printability characteristics and biocompatibility and is primarily derived from two sources: plant matter and bacterial biosynthesis (Lin & Dufresne, 2014), however, more recently, tunicates have proven to be an additional source of this material (Dunlop et al., 2020). Of the plant-derived types, the material is typically available as nanocrystals or nanofibrils; though a blended morphology has recently been described, comprising a naturally-derived combination of the two structural formulations (Al-Sabah et al., 2019; Jessop et al., 2019 ; Kyle et al., 2018). We have previously characterised plant-derived nanocellulose fibrils, crystals and blend formulations derived through "American Value Added Pulping" (AVAP®) technology, which yields nanocelluloses with enhanced thermal stability, owing to the absence of sulphate substitution to functional side chains that occurs with conventional sulphuric acid hydrolytic processing (Nelson & Restina, 2014). Through a combination of scanning electron microscopy, transmission electron microscopy, atomic force microscopy and rheology, each material demonstrated extensive porosity at the micro and nanoscale, in addition to excellent thermal stability (Kyle et al., 2018). Rheologically, each of the nanocellulose formulations have been demonstrated to offer shear thinning behaviour rendering them suitable for extrusion-based 3D printing and a dominance of elastic type behaviour with a G' greater than G'' (Jessop et al., 2019; Kyle et al., 2018) (Supplementary Fig. 4). However, disparities in micro- and nanoarchitecture were identified between the crystal (NCC), fibril (NFC) and blend (NCB) variants, specifically where pore size, viscosity and rigidity were interrogated (Kyle et al., 2018) (Supplementary Figs. 1–3). These disparities may have implications at a cellular level especially considering the micro- and nanoscale at which cell-material interactions may be occurring (Al-Sabah et al., 2019). Yet, to date there have been no studies that have compared the effects of these structural differences on the ability to effectively generate 3D bioprinted cartilage constructs: in particular when considered from a perspective of not only printability but also chondrogenesis. As such, we hypothesise that the structural disparities between nanocellulose crystals, fibrils and blend bioinks would translate to biological differences in chondrocyte behaviour with implications for cartilage tissue engineering.

It is essential to address this potential alongside the mechanical and structural characterisation to fully evaluate the suitability of this promising candidate bioink for 3D bioprinting cartilage tissue. In doing so, it is hoped that this study will direct research into most suitable nanocellulose derivative(s) for the next generation of translatable nanocellulose composite bioinks for bioprinting human cartilage.

2. Methods

2.1. Cell culture and isolation

Human nasoseptal chondrocytes (hNSCs) were isolated from excess nasoseptal cartilage discarded from septorhinoplasty procedures with informed patient consent (Ethical approval granted by Research Ethics Committee, National Institute for Social Care and Health Research, Welsh Government, IRAS ID 99202). Cartilage tissue was diced into 1 mm^3 pieces in aseptic conditions and digested in 0.4 % pronase (Roche, UK) for 1 h at 37 °C, 5 % CO_2 with gentle agitation, followed by secondary digestion in 0.2 % collagenase type I solution for 16 h (Sigma-Aldrich, Poole, UK). The resultant cell suspension was filtered through a 40 μm cell strainer (Corning, NY, USA) and centrifuged at 350*g* for 6 min. Cells were cultured in 5 % CO_2 at 37 °C with culture medium changed every 2–3 days. Culture medium comprised Dulbecco's Modified Eagle Medium without glucose (Sigma-Aldrich, Poole, UK) supplemented with 10 % fetal bovine serum (Sigma-Aldrich, Poole, UK), 100 μg/ ml penicillin and 100 U/ ml streptomycin (Sigma-Aldrich, Poole, UK), 1 mM glucose (SigmaAldrich, Poole, UK), and 0.1 % non-essential amino acids (Thermo Fisher Scientific, Paisley, UK). Cells were grown to 70 % confluence and passaged using 0.05 % trypsin-EDTA (Thermo Fisher Scientific, Paisley, UK). Cell number was calculated using a trypan blue exclusion assay (Thermofisher Scientific, MA, USA). Cells were used at passage 2 using primary cell lines derived from 3 separate biological repeats (patients).

2.2. Nanocellulose bioink production and formulation

American Value Added Pulping Corporation "AVAPCO" (Thomaston, Georgia, USA) provided the BioPlus® nanocellulose particles that were produced from raw wood chip biomass using AVAP® technology, which fractionates the biomass into cellulose, lignin and hemicelluloses using ethanol and sulphur dioxide as previously described (Nelson & Restina, 2014). The resultant nanocellulose formulations are NCC gel (Nanocrystalline Cellulose, pure cellulose, 3 % w/v), NFC gel (Nanofibrillar Cellulose, 6 % w/v) and NCB gel (Nanocellulose Blend, 3 % w/v) in water and have been extensively characterised structurally in our previous work (Kyle et al., 2018) (Supplementary Material A). 50 ml of each formulation was centrifuged at 1500*g* for 5 min and the liquid supernatant discarded. Sodium alginate (from brown algae, 80,000–120,000 Da, medium viscosity, 2 % at 25 °C, Sigma-Aldrich, MO, USA) was UV sterilised in powder form and dissolved in sterile, tissue culture grade water to produce a 2.5 % (w/v) solution as previously optimised and described (Al-Sabah et al., 2019; Jessop et al., 2019). Our previous work has optimised the concentrations and proportions of AVAP-derived nanocelluloses and alginate which were replicated for this study (Al-Sabah et al., 2019; Jessop et al., 2019; Kyle et al., 2018). In brief, 75 ml of each nanocellulose biomaterial was made into a composite bioink through the addition of 25 ml of the 2.5 % (w/v) sodium alginate solution, as previously described. The composite bioink was then homogenised using a stirrer and syringe and autoclaved at 100 kPa, 121 °C for 45 min and corrected to pH 7.4 through the dropwise addition of 1 M sodium hydroxide solution. Each nanocellulose composite bioink was compared to the 2.5 % (w/v) alginate solution alone as a control.

A cell-biomaterial suspension of 3×10^6 cells per ml was produced and used to dispense 100 μl semispheres of biomaterial for chondrogenicity and biocompatibility assessments (Sections 2.4, 2.5, 2.6, 2.8 and 2.9). The constructs were crosslinked using 0.5 M calcium chloride as previously optimised and reported (Al-Sabah et al., 2019) for 5 min and thereafter washed with warm phosphate buffered saline (PBS) solution. The diameter of the semispheres was measured using digital callipers prior to the application of crosslinker and repeated after the wash with PBS. A percentage change in construct diameter was used to assess swelling post-crosslinking. Constructs were immersed in media as outlined above and cultured for up to 1 month at 37 °C and 5 % CO_2 with media changes performed every 3 days.

2.3. Printability assessments

A CELLINK™ INKredible bioprinter (CELLINK, Gothenburg, Sweden) was used to test the printability characteristics of the different nanocellulose formulations. The printer was connected to an air compressor and set to 300 kPa. The printheads were calibrated to 0 kPa and the nozzles opened through the printer control system. The minimum extrusion pressure was determined by slowly increasing the pressure of each printhead until bioink is extruded through the 22G nozzle as a continuous filament.

Cellink Heartware software (Version 2.4.1, CELLINK, Gothenburg, Sweden) was used to design the 3D shapes for extrusion bioprinting within the parameters of the print bed area. 3D shapes for printing were designed ab initio using the software and saved as .STL (stereolithography) files, or 3D design software packages including Autodesk (Autodesk, CA, USA) and Windows 3D Viewer (Microsoft, WA, USA). The 3D shapes created were then converted into vertical layer by layer instructions in the form of .gcode files through the use of Slic3r software (v3, GitHub, CA, USA). This software was also used to refine the printer settings including infill pattern (rectilinear), infill density (80 %), print speed (12 mm^3/s), layer height (0.2 mm), temperature (23 °C) and supporting frameworks. Next, the ability of the inks to be printed in a continuous straight line was determined as a measure of resolution. These lines were thereafter examined under light microscopy and measured using Olympus CellSens software (Olympus, Japan) at a minimum of three points. Once optimised, 3D shapes were produced using Autodesk (Autodesk, CA, USA) of increasing complexity from 2D grids to 3D prisms, and finally constructs resembling anatomical structures: tracheal rings and an auricular antihelix. Digital callipers were used to measure set points in the constructs to determine the uniformity of the structures. Measurements were compared to a 'gold standard' model printed in poly-lactic acid (PLA) using an Ultimaker 3 (Ultimaker, Utrecht, Netherlands) printer as a control.

2.4. Chondrogenic gene expression

In order to quantify gene expression, triplicates of each biomaterial were uncrosslinked using Ethylenediaminetetraacetic acid (EDTA) solution (Sigma Aldrich) and TRIzol (Invitrogen, Thermofisher) and subsequently degraded with a TissueRuptor II probe for 30 s (Qiagen, Germany). The lysate was processed using Qiagen QIAshredder and RNeasy Mini Extraction kits (Qiagen, Germany) to yield ribonucleic acid (RNA) for reverse transcription. The RNA was quantified and assessed for purity, converted to complementary deoxyribonucleic acid (cDNA) through reverse transcription quantified for the expression of Type 2 Collagen (COL2A1), SOX9 and Aggrecan (ACAN1) relative to housekeeping gene expression (RPL13A and TBP) using real time quantitative polymerase chain reaction (PCR) (CFX Connect Realtime PCR detection system, Bio-Rad). Each material was harvested for RNA extraction and PCR analysis at 4 h, 7 days, 14 days and 21 days of culture. All relative gene expression values were expressed as fold-changes using the $^{\Delta\Delta}$CT method (Livak & Schmittgen, 2001) compared to alginate at the 4-hour time point.

2.5. Extracellular matrix quantification

The dimethylmethylene blue (DMMB) assay was used to quantify glycosaminoglycan (GAG) content in each material at 7 days and 21 days of culture. The cell-laden biomaterial semispheres of each bioink were lysed to yield protein isolates for GAG quantification. Isolates were diluted 1 in 50 with distilled water to which DMMB reagent was added. The plates were read immediately at 525 nm using a plate reader (POLARstar Omega spectrophotometer, BMG LABTECH, Ortenberg, Germany) and compared to a series of chondroitin standards ranging from 0 to 50 μg/ml.

2.6. Histological analysis

To determine the arrangement of ECM relative to the cells within the biomaterials, histological analysis was performed. Cell-laden biomaterial semispheres were immersed in 4 % paraformaldehyde solution for 30 min and then washed three times in PBS. The constructs were then immersed in 1 % (w/v) Alcian Blue stain, washed sequentially with hydrochloric acid and distilled water until no further stain was released. Constructs were viewed under brightfield microscopy at 4, 10 and 20× magnification using a CKX53 Microscope (Olympus, Japan). Images were taken throughout the construct (in x, y and z axes) using CellSens Software (Olympus, Tokyo, Japan) to ensure the images captured were representative of the whole material.

2.7. Mechanical compression

The break force, strain and ultimate compressive strength of the constructs were determined using a mechanical compression device (1ST, Tinius Olsen). 100 μl cylindrical disks were produced of equal dimensions (8 mm diameter) and added to the base plate of the compressor. The upper plate was lowered to within 1 mm of the biomaterial disk and upon achieving a contact pressure of 0.01 N, compression was initiated at a rate of 2 mm/min until the material fractured. The break force, distance and ultimate force applied were recorded initially without cells, and thereafter following 21 days of culture with hNSCs.

2.8. AlamarBlue assay

To determine cell viability, proliferation and metabolic activity, an alamarBlue Assay was performed at 4 h and 7, 14 and 21 days. The media was removed from the well and replaced with media supplemented with 10 % alamarBlue dye (v/v) for 4 h. Samples of the alamarBlue media were then transferred in triplicate from each well to a 96 well plate along with alamarBlue media only controls. The colorimetric change was quantified using a plate reader (POLARstar Omega spectrophotometer, BMG LABTECH, Ortenberg, Germany) in which absorbency readings were taken at 570 nm (reduced form) and 600 nm (oxidised form) wavelengths. The percentage of reacted alamarBlue reagent was calculated relative to the media only controls.

2.9. Live-dead assay

A live dead mammalian cell viability assay kit (Thermofisher Scientific, MA, USA) was used to visualise live and dead cells within the biomaterials. Media was discarded from the cells and pellets and washed in PBS. A 1:1000 Calcein-AM dye and 1:500 Ethidium homodimer-1 solution was added for 45 min, protected from light, and washed with PBS. The constructs were visualised using inverted fluorescent microscopy for live and dead cells at 4 and 10-times magnification.

2.10. Statistical analysis

All data sets were assessed for normality using the Anderson Darling

test and technical triplicates performed for each condition. Printability assays were compared using Brown-Forsythe ANOVAs, relative gene expression with two tailed *t*-tests and a 2-way ANOVA to compare material characteristics. Unless otherwise stated, graphical depictions of datasets represent mean values with standard deviation. A set of three biological repeats were performed for all cell-based experiments and a minimum of three technical triplicates were performed for all experiments.

3. Results and discussion

3.1. Bioink printability

The inclusion of all formulations of nanocellulose in the bioinks was found to significantly improve printability. Despite having the lowest printing pressure (3 kPa), the alginate demonstrated poor fidelity and post-printing stability rendering it unsuitable for 3D printing at the viscosity (2.5 % w/v) used in this study mirroring the findings of previous assessments of alginate printability (Freeman & Kelly, 2017; Hazur et al., 2020; Jessop et al., 2019). Alginate bioinks vary in their printability characteristics depending on the molecular weight, viscosity and concentration of the bioinks but research to date has highlighted poor post-printing shape fidelity as a recurring and persistent issue with inks based in this material, particularly at low concentrations (<3 % w/v) (Piras & Smith, 2020). A benefit of low viscosity bioinks is the low extrusion pressures needed to facilitate flow through a nozzle (Kyle et al., 2017), which is likely to offer superior cell viability during the printing process owing to lower amounts of shear stress exerted upon the cells (Axpe & Oyen, 2016). Lower concentration alginate bioinks have also been demonstrated to augment chondrogenic gene expression in 3D culture, to a greater degree than higher concentration formulations (Ewa-Choy et al., 2017). Previous work by Jessop et al, demonstrated that whilst 2.5 % (w/v) alginate demonstrates almost Newtonian-type fluid behaviour, there was limited shear thinning at 5 % (w/v) and above, with all alginate bioinks demonstrating a dominance of viscosity (G″) over elasticity (G′) (Jessop et al., 2019). In isolation, alginate hydrogels of low or high concentration therefore appear to be met with either poor chondrogenicity or poor printability respectively, neither of which are acceptable for cartilage tissue engineering purposes.

As such, nanocellulose was introduced to the bioink to enhance printability (Table 1). In doing so, the extrusion pressure of the nanocellulose based inks was expectedly higher than pure alginate hydrogels. Of the nanocelluloses used, the NFC had the lowest extrusion pressure (5 kPa), followed by the NCB (7 kPa) and lastly the NCC (10 kPa). Nanocellulose-alginate bioinks, demonstrate shear thinning, non-Newtonian type viscoelastic behaviour in contrast to pure alginate bioinks. NFC in particular, has been previously credited for its shear thinning capabilities, as the nanocellulose fibrils can disentangle and align parallel to the direction of flow at lower shear rates, which may account for the lower extrusion pressures observed (Jessop et al., 2019; Markstedt et al., 2015).

3.1.1. Bioink resolution and shape fidelity

All nanocellulose materials displayed satisfactory printing resolution using the straight-line assay (Fig. 1), with NFC capable of the greatest resolution (0.6 mm ±0.13) compared to NCB (0.68 mm ±0.27) and NCC (0.84 mm ±0.46). There were no significant differences in the mean line diameter generated by the biomaterials when printed ($p = 0.57$). However, a much greater range of values was observed in the NCC lines (SD = 0.46 mm) than NCB (SD = 0.27 mm) and NFC (SD = 0.13 mm) indicating a greater degree of line width consistency was achieved in the NFC prints.

Each nanocellulose bioink was thereafter used to print a simple grid or lattice comprising 5 horizontal and 5 vertical lines, yielding 25 square spaces (Fig. 2). The NFC displayed the tightest range of peripheral border sizes (0.50 mm), compared to NCB (1.04 mm) and NCC (1.49 mm) but the NCB had the best reproducibility in grid sizes with a more consistent mean grid area (8.4 mm^2), closer in area to the plastic control (9 mm^2) when compared to NFC (6.9 mm^2) and NCC (7.9 mm^2). However, these were not significantly different measurements ($p = 0.94$) between bioinks.

All nanocellulose materials were able to produce rings consistent with the 3D design (Fig. 1). All constructs were thicker at their minimum and maximum widths than the 3D design by a mean of 1.775 (NCB), 0.725 (NFC) and 1.205 mm (NCC) but this was not statistically significant ($p = 0.5$). As with the other assays, there was a greater range of thicknesses observed in the NCC (range = 1.33 mm) and NCB (range = 1.03 mm) prints than the NFC (range = 0.09 mm), the latter of which displayed greater uniformity and consistency throughout the prints.

Reproduction of a human auricular antihelix was achieved with each nanocellulose-alginate bioink (Fig. 4), however the NCB offered the most consistent measurements in this test compared to the plastic control (mean difference = 0.424 mm ±1.68), followed by NFC (0.526 mm ±2.17) and NCC (−1.234 mm ±3.44). No material was found to be significantly different to the plastic control measurements however indicating satisfactory shape fidelity was achieved ($p > 0.99$ for all comparisons). There were additionally no statistically significant differences between the NC bioinks ($p = 0.52$).

Low viscosity bioinks such as the 2.5 % alginate used in this study offer a low extrusion pressure but with the caveat of inadequate tensile strength to hold their shapes after printing (Freeman & Kelly, 2017), and all attempts to print grids, rings and antihelical structures were unsuccessful with alginate alone. However, when blended with nanocelluloses, the printability of 2.5 % alginate was found to be markedly improved, consistent with previous studies of nanocellulose-alginate printability assessments (Jessop et al., 2019; Müller et al., 2017).

All nanocellulose subtypes: NCC, NFC and NCB demonstrated satisfactory post-printing shape fidelity as demonstrated by successful prints for lines, grids, rings and antihelices. Indeed, the NFC and NCB nanocelluloses performed more consistently in most of the printability studies tested in than NCC, with the NFC demonstrating the lowest degree of intra-print variation in the line fidelity and ring assays, whilst the NCB demonstrated measurements closest to the intended construct size in the antihelix and grid assays. The ability of cellulose nanostructures to disentangle during printing and entangle post-printing is mirrored in its rheological properties: shear thinning during the printing process and a recovery in the storage modulus post-printing (Jessop et al., 2019; Torres et al., 2012). These properties are a phenomenon of nanocelluloses, in which the anisotropic particles within the polymer orientate under pressure (such as extrusion pressures in bioprinting) and self-assemble in the directionality of printing (Ma et al., 2021), translating to excellent printability properties such as fidelity and resolution. However, there is a discrepancy in the inks when comparing their resolution to their shape fidelity: superior resolution was achievable with the NFC bioink in the line assay, whereas the fidelity was superior in the NCC and NCB bioinks. Based on previous transmission electron microscopy analysis of the nanocellulose variants, this superior post-printing resolution in the NFC and the NCB, may reflect the nanostructure of the fibrillar component, in which a greater degree of entanglement between long nanofibrils was observed compared to the crystalline variants,

Table 1
Overall performance of bioinks tested in this study for extrusion pressure, resolution, and fidelity assays. - = unsuitable; + = possible; ++ = good; +++ = excellent.

Material	Mean printing pressure (kPa)	Line assay	Grid assay	Ring assay	Anatomical fidelity assay
Alginate	3	+	–	–	–
NCB	7	++	+++	++	+++
NCC	10	++	++	++	++
NFC	5	+++	++	+++	+++

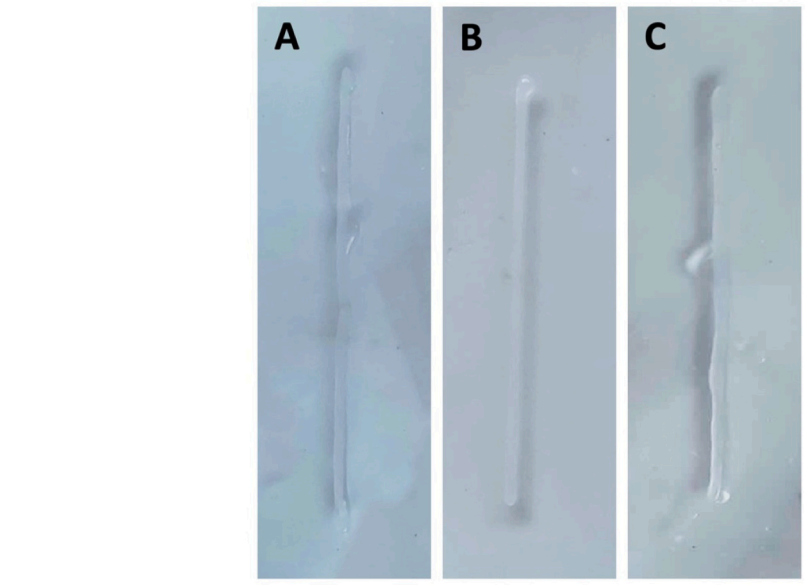

	NCB	NCC	NFC
Mean line width (mm)	0.68	0.84	0.60
Std dev	0.27	0.46	0.13
Range	0.64	0.83	0.28

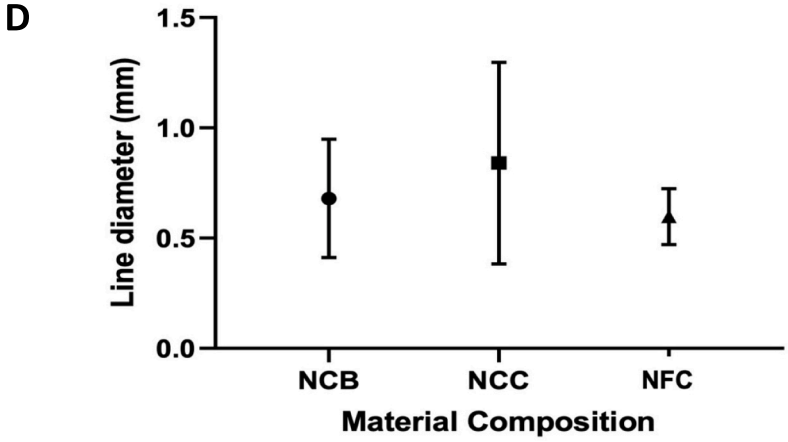

Fig. 1. Line resolution assay comparing NCB (A), NCC (B) and NFC (C). Representative images of each line are displayed (A–C) with the mean measurements ($n = 3$) of each line, the standard deviation and range displayed beneath. The mean line width values plus range (in mm) are depicted graphically in (D), demonstrating a smaller range and narrower line in NFC compared to NCB and NCC. No statistically significant differences were observed between the mean line thicknesses.

facilitating superior alignment of fibrils in the direction of flow and shape retention through increased hydrogen bonding (Jessop et al., 2019; Kyle et al., 2018).

3.1.2. *Effect of crosslinking on post-printing shape fidelity*

Despite demonstrating good post-printing fidelity, each biomaterial was noted to undergo swelling after immersion in crosslinking agent (Fig. 5). The diameter of the nanocellulose materials was compared before and after immersion in crosslinking agent to determine changes in construct size as a result of the crosslinking process. Comparable swelling properties were observed with each of the nanocellulose materials, with a lowest mean swelling in the NCC (3.2 %) and NCB materials (6.6 %) and highest in the NFC (9.9 %). Structurally, the network of NCC demonstrates compact nanorods packed together with relatively low porosity, in contrast to the fibrils which form complex entanglements in the micro to nano scale, and NCB which contains both porous fibrillar elements and compact nanorods that more closely resemble bacterial nanocellulose (Kyle et al., 2018). Furthermore, the nanocelluloses used in this study are known to have a negative zeta potential (surface charge) of approximately −23.3 mV from previous characterisation, rendering them hydrophilic (Kyle et al., 2018). The structural properties of these formulations underpin the affinity to absorb water from the crosslinking agent, and may as such reflect the degree of swelling the constructs undergo as a result of immersion in crosslinking solution. Nonetheless, the swelling observed further exacerbates the deviation of the 3D bioprinted constructs from the intended dimensions of the constructs, seen most markedly in the NCB and NCC shape resolution post-printing (Figs. 2–4). The interactions of porosity, crosslinking and shape fidelity should as be factored into future computer aided designs, particularly where constructs requiring anatomical mimicry are planned.

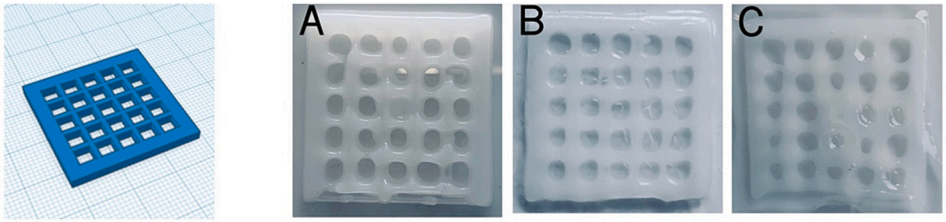

	NCB	NCC	NFC
Intended line width (mm)	3	3	3
Mean line width (mm)	2.79	2.83	2.72
Range of line widths (mm)	0.89	0.63	0.19
Intended grid area (mm^2)	9	9	9
Mean grid area (mm^2)	8.4	7.9	6.9
Mean Area Discrepancy (mm^2)	0.6	1.1	2.1

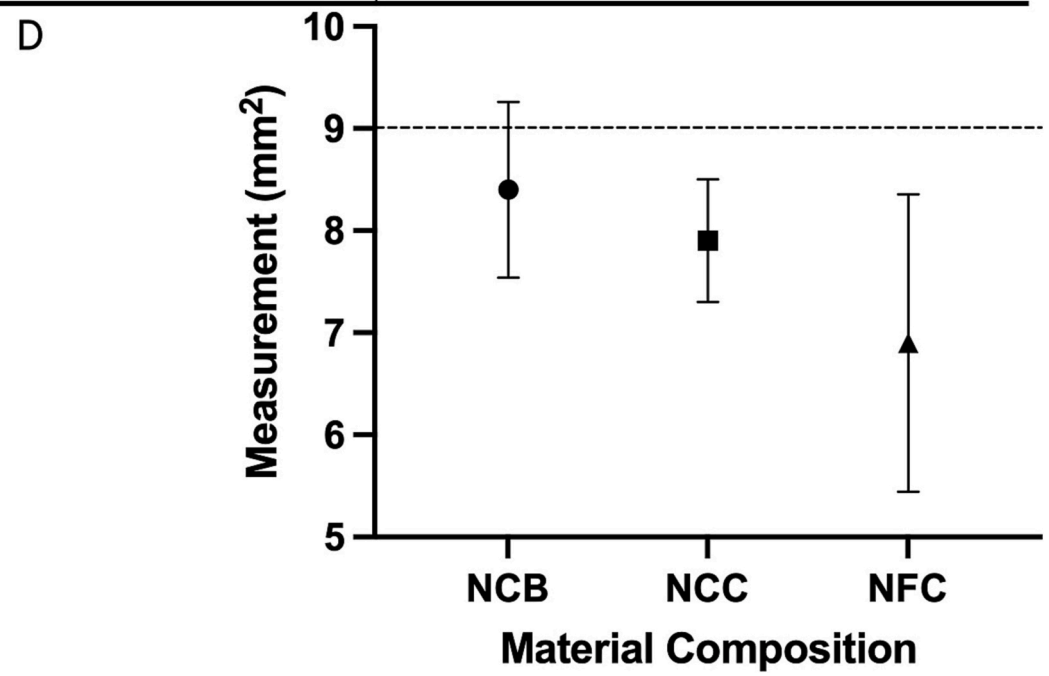

Fig. 2. Grid Assays and their measurements printed with representative images of NCB (A), NCC (B) and NFC (C). Three grids per material were printed and the mean grid area taken from a minimum of 3 grids. The ranges and deviation from the intended grid geometry is presented in the table and the mean grid area and standard deviation is graphically depicted in (D). A dotted horizontal line represents the intended grid area of 9 mm^2 reference.

3.2. Chondrogenic gene expression in nanocellulose and alginate bioinks

Chondrogenic gene expression was observed over a 21-day time course to determine expression of the chondrogenic hypertrophy gene (SOX9) and the expression of cartilage-specific ECM genes: type 2 collagen (COL2A1) and aggrecan (ACAN1). All results were compared to alginate at 4 h as a control to determine the temporal relationship in relative gene expression.

All nanocellulose-based materials demonstrated increases in chondrogenic gene expression over the course of 21 days, but the most marked rises were in NCC for all genes, with NCB and NFC also demonstrating significant rises in SOX9 and ACAN1/COL2A1 gene expression respectively. All materials demonstrated biologically relevant (>1.5×) increases in COL2A1 expression at and beyond 4 h compared to alginate alone, with statistical significance achieved in the NCC (405.7-fold increase, $p < 0.0001$) and NFC (302.1-fold increase, $p = 0.0003$) materials at 14 days. In NCC, the gene expression of COL2A1 had risen by 1580-fold greater expression ($p < 0.0001$) by 21 days. ACAN1 expression demonstrated a similar temporal relationship, increasing in NCC at all time points, with statistically significant increases in gene expression seen at 14 days (31-fold, $p = 0.0017$) and 21 days (36.7-fold, $p = 0.0006$). NFC had a significantly higher expression of ACAN1 at 14 days ($p = 0.0039$) but no other time points. With regards to SOX9, a statistically significant elevation of expression was observed in NCB (1.7-fold, $p < 0.0001$) and NCC (1.4-fold, $p = 0.0005$) as early as 4 h and at 14 days in NCC (4.9-fold, $p = 0.0041$).

Whilst increases in the relative gene expression of alginate were observed over the 21 days, with the exception of a modest significant rise in SOX9 at 7 and 14 days, none of the gene expression changes were statistically significant relative to the initial time point. Previous studies of alginate chondrogenicity have been explored using mesenchymal stem cells (MSCs) and demonstrated significant rises in type 2 collagen, SOX9 and ACAN1 over 21 days relative to cells cultured in 3D pellet or 2D monolayer conditions (Dashtdar et al., 2016; Yang et al., 2004).

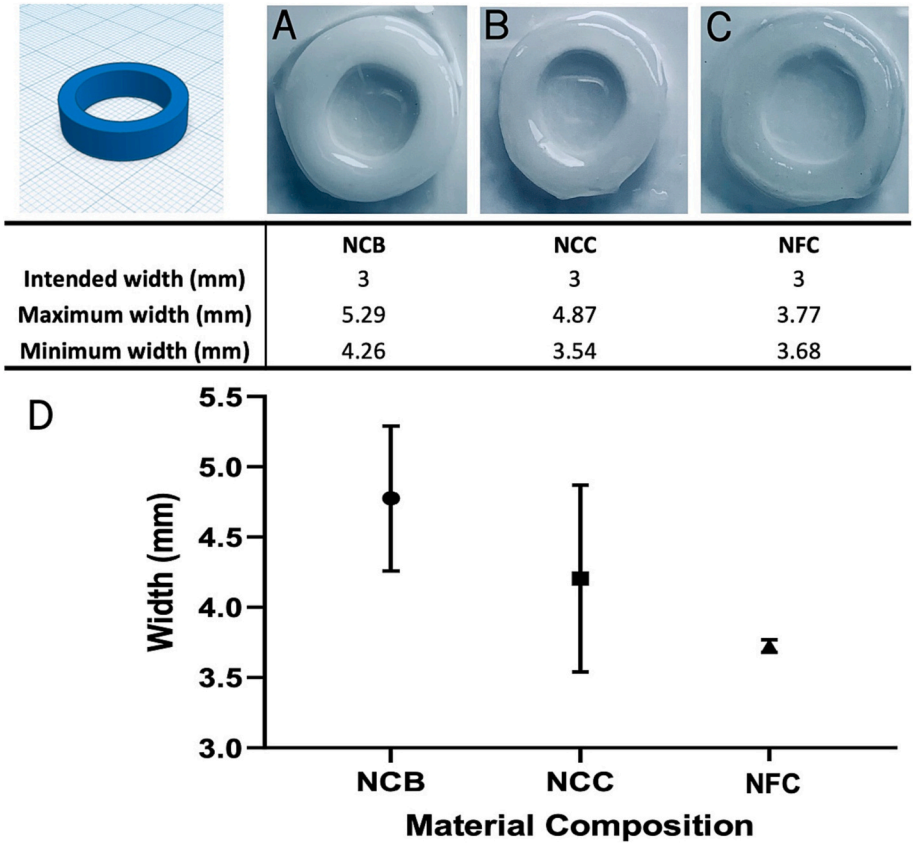

	NCB	NCC	NFC
Intended width (mm)	3	3	3
Maximum width (mm)	5.29	4.87	3.77
Minimum width (mm)	4.26	3.54	3.68

Fig. 3. Representative images of circular rings printed using NCB (A), NCC (B) and NFC (C) are displayed with mean measurements of tracheal ring thickness taken from least 3 points per ring (D). Error bars depicting the range are displayed. No significant differences were observed between mean ring thicknesses ($p = 0.5$).

These studies emphasise the advantageous nature of hydrogels for chondrocyte cell culture, attributable to superior mimicry of the in vivo extracellular matrix environment (Tibbitt & Anseth, 2009). This study, however, expands on this to demonstrate that alginate is not inherently chondrogenic, particularly in comparison to nanocellulose-alginate bioinks in which overt evidence of enhanced chondrogenic gene expression was observed. Indeed none of the previous studies of nanocellulose-alginate include a comparison of chondrogenic gene expression relative to pure alginate (Martínez Ávila et al., 2015, 2016; Möller et al., 2017; Müller et al., 2017) making this study the first direct comparison between these materials using primary human chondrocytes.

Structurally, nanocellulose may promote a more chondrogenic environment than alginate owing to superior ECM mimicry, and both nano- and micro-roughness, which may evoke superior cell adhesion and direct chondrogenic differentiation (Kyle et al., 2018). Bacterial nanocellulose-alginate scaffolds have been reported to offer chondrogenicity with human nasoseptal chondrocytes previously, with increases in ACAN1, COL2A1 and COL1A1 gene expression seen over a course of 6 weeks (Martínez Ávila et al., 2015). The increases observed with bacterial nanocellulose however were not statistically significant, and not compared to alginate alone, in contrast to the stark and highly significant increases observed with pulp-derived nanocelluloses in our study.

This comparative gene expression analysis complements the printability data to demonstrate that not only is nanocellulose superior in printability, but it additionally confers a biological advantage of enhanced chondrogenicity over alginate.

Between nanocellulose subtypes, NCC was the formulation evoking the most favourable gene expression profile for chondrogenesis, with significant elevations in COL2A1 and ACAN1 relative to alginate at 4 h and higher fold-changes than the other formulations. The compact, homogeneous nature of the crystalline subtype may offer a closer structural mimicry of the compact and regular arrangement of glycosaminoglycans such as hyaluronic acid and chondroitin sulphate, whereas the fibrillar arrangement may match the anisotropy of the collagen bundles found in cartilage tissue ECM (Han et al., 2011). This could certainly explain why the NCC and NFC appeared to have high increases in ACAN1 and COL2 expression over 21 days. It might be expected however, that the NCB, containing both the crystalline and fibrillar elements, may therefore even better emulate the structure of cartilage ECM. The NCB evoked the highest fold-change in SOX9 expression at the 7-day time point but this did not otherwise translate to advantageous gene expression profiles. SOX9 is a marker of chondrocyte differentiation, survival and an upregulator of ECM genes (Lefebvre et al., 2019). However, where NCB is concerned, the rise in SOX9 failed to translate to a subsequent rise in the expression of ACAN1 and COL2A1, which may have fallen beyond the duration of the experimental period (see Fig. 6).

3.3. Extracellular matrix formation in nanocellulose bioinks

Glycosaminoglycan (GAG) content was quantified using the DMMB assay at 7 and 21 days of culture in each biomaterial. All of the biomaterials studied demonstrated a statistically significant increase in GAG content from 7 to 21 days ($p < 0.0001$) with a mean increase of 832.1 μg/ml (±46.39). At 21 days the highest GAG content was observed in the NCC material (1434 μg/ml) though no statistically significant differences were observed between biomaterials ($p = 0.091$).

The cell-laden biomaterials were stained with Alcian Blue stain to visualise cell density, arrangement, pericellular and extracellular matrix production. Extracellular matrix was readily stained in each of the

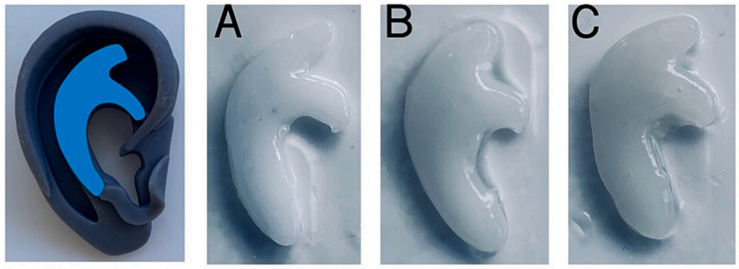

	Intended size (mm)	NCB (mm)	NCC (mm)	NFC (mm)
Length	*33.29*	31.72	27.61	30.72
Width	*18.32*	17.36	14.13	17.42
Body	*5.64*	6.66	7.5	8.22
Superior crus	*5.77*	6.82	6.89	7.59
Inferior crus	*3.6*	6.18	4.32	5.3
Mean deviation	-	0.424	-1.234	0.526

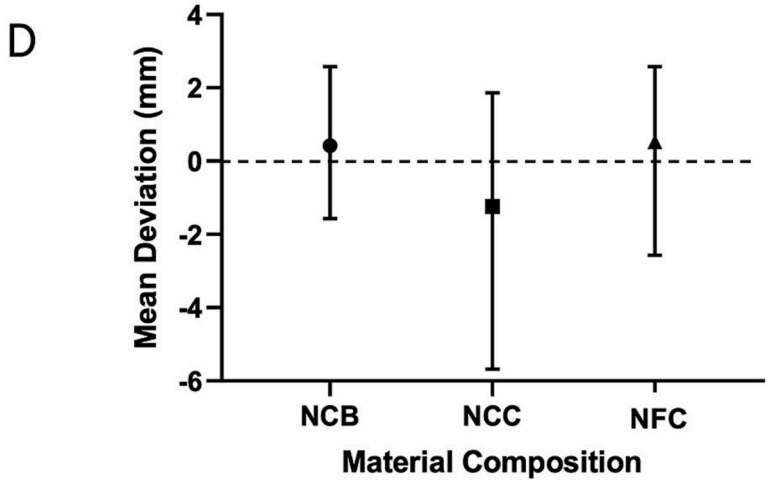

Fig. 4. Representative images of antihelices printed with NCB (A), NCC (B) and NFC (C). A recognisable antihelix was reproducible with all nanocellulose subtypes but NCB had the lowest amount of deviation from the intended parameters of the antihelical design as demonstrated in the table and graphically in (D). A dotted line on (D) is used to depict the point of no deviation in size from printing in plastic; mean values of 3 repeats with error bars depicting the range are presented. No statistically significant differences were noted between bioinks or compared to plastic.

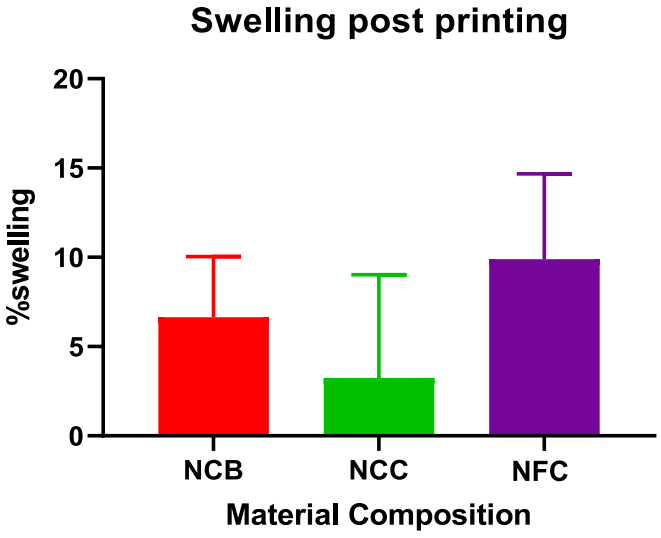

Fig. 5. Swelling of nanocellulose bioinks after printing and crosslinking application expressed as a percentage of the original size post-printing. The mean values of each material are presented with error bars depicting standard deviation ($n = 6$). No statistically significant differences were observed between materials.

biomaterials studied (Fig. 8). The greatest number of cells could be visualised in the NCB material in which there was also evidence of intense extracellular matrix staining. This indicates the matrix has been deposited by cells within the material rather than non-specific staining to the material as evidenced in Fig. 8C. The cells visualised through histological analysis appear to exist in isolation surrounded by a rim of matrix as seen in native cartilage lacunae. This phenomenon was also observed, albeit to a lesser degree, in the NCC, NFC and Alginate materials (Fig. 8A, C & D) however there was variable uptake of stain around cells in the alginate material, with many not staining for GAG production (Fig. 8A). Histologically, it would therefore appear that all nanocellulose materials demonstrate ECM staining, consistent with the DMMB assay. Whilst chondrocytes cultured in alginate also appeared to produce GAGs (Fig. 7), this did not appear to be deposited in a pericellular environment as overtly or uniformly as in the nanocelluloses.

3.4. Biomechanical properties of bioinks

3.4.1. Biomechanical properties in the absence of chondrocytes

Each of the biomaterials was tested mechanically for their deformation and strength using uniaxial compressive loading (Fig. 9). The ultimate compressive stress (UCS), break force and strain to failure experienced by the biomaterials were also recorded and compared across materials (Fig. 10). It was noted that NFC had a significantly lower UCS (0.14 MPa, $p = 0.029$) than alginate alone (0.76 MPa), but that there were no significant differences between alginate and NCC

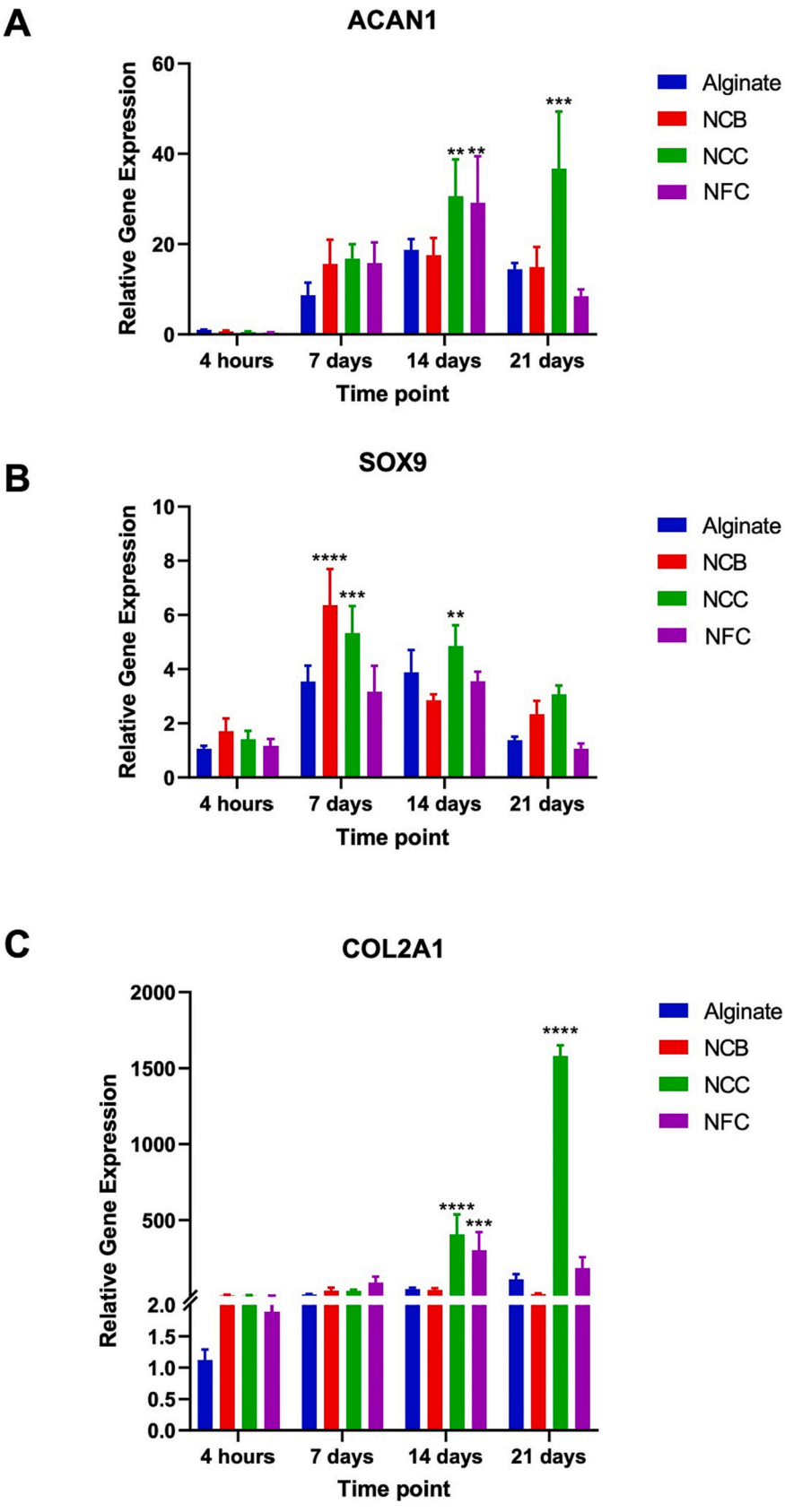

Fig. 6. Chondrogenic gene expression profile over 21-day time course. All relative gene expression values displayed represent a mean of three biological repeats (performed in at least technical triplicates) with standard error, relative to alginate at 4 h. A) Aggrecan gene expression profile at 4 h, 7 days, 14 days and 21 days in culture. All values were biologically significant (>2) after 7 days but only statistically significant in NCC (14 days, 21 days) and NFC (14 days). B) SOX9 gene expression profile over 21 day time series. All bioinks produced biologically significant differences in SOX9 expression relative to 4 h at 7 and 14 days with the highest peak achieved in NCB at day 7. C) Type 2 collagen gene expression profile over 21 days. Biologically significant increase in type 2 collagen were observed after 7 days but significant in NCC (14, 21 days) and NFC (14 days) only. * = $p < 0.05$; ** = $p < 0.01$; *** = $p < 0.001$; **** = $p < 0.0001$.

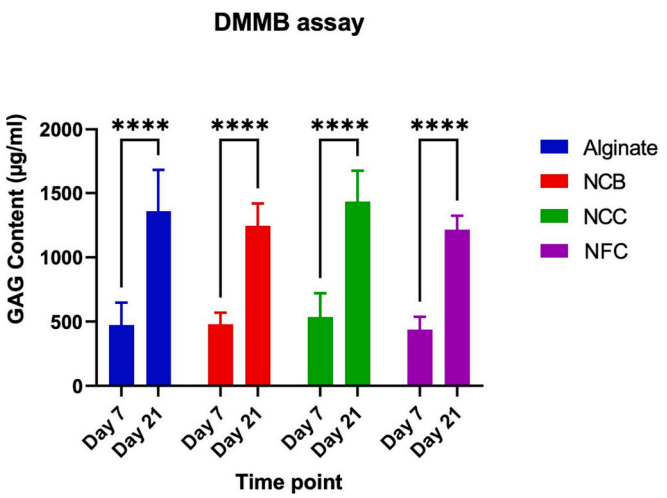

Fig. 7. Dimethylmethylene blue (DMMB) assay to quantify glycoasminoglycan (GAG) content in nanocellulose and alginate bioinks at 7 and 21 days of culture. The mean value of 9 repeats (technical $n = 3$, biological n = 3) is presented with error bars of standard deviation. Significant increases were observed in all biomaterials between the two time points, however no statistically significant differences in GAG content were observed between the materials at Day 7 or Day 21. **** = p < 0.0001.

(0.20 MPa, $p = 0.45$) or NCB (0.24 MPa, $p = 0.99$).

Strain to failure was comparable across all biomaterials: Alginate (75.5 %), NCB (78.7 %), NCC (69.7 %) and NFC (68.2 %). These were not statistically significant differences ($p = 0.35$). A higher break force was achieved with alginate (4.99 N) than the other nanocellulose materials, of which NCB had the highest break force (1.49 N, $p = 0.34$) and NFC was significantly lower than alginate (0.59 N, $p = 0.006$). No other significant differences were observed between the nanocellulose biomaterials. As such, the compression testing indicates that the alginate alone has the most robust mechanical compression properties compared to the nanocellulose-alginate composite bioinks, and that of the nanocellulose-based bioinks, NFC is structurally the weakest formulation under compressive load.

3.4.2. *Biomechanical properties following culture with hNSCs*

Whilst the alginate material was consistently stronger than the nanocellulose-alginate composite bioinks in terms of UCS (Fig. 10A), there was no significant change following the addition of cells (0.76 MPa, $p = 0.07$). The NCB demonstrated the most significant increase in UCS from 0.24 to 0.53 MPa ($p = 0.004$), but NCC (0.49 MPa, p = 0.02) and NFC (0.27 MPa, p = 0.02) also demonstrated significant increases

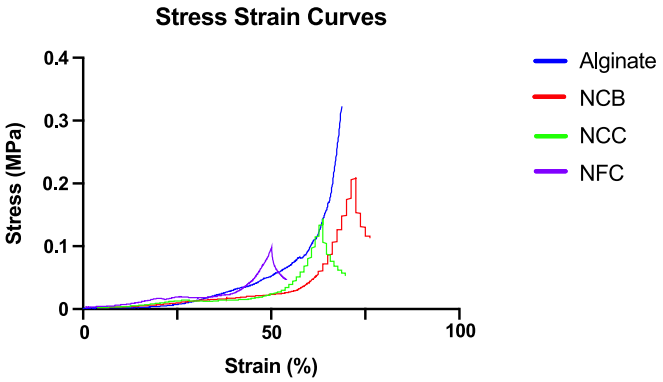

Fig. 9. Stress-strain curves of Alginate, NCB, NCC and NFC under uniaxial compressive loading. Stress in MPa is plotted against Strain (%) to material failure. Representative curves from triplicate repeats are demonstrated.

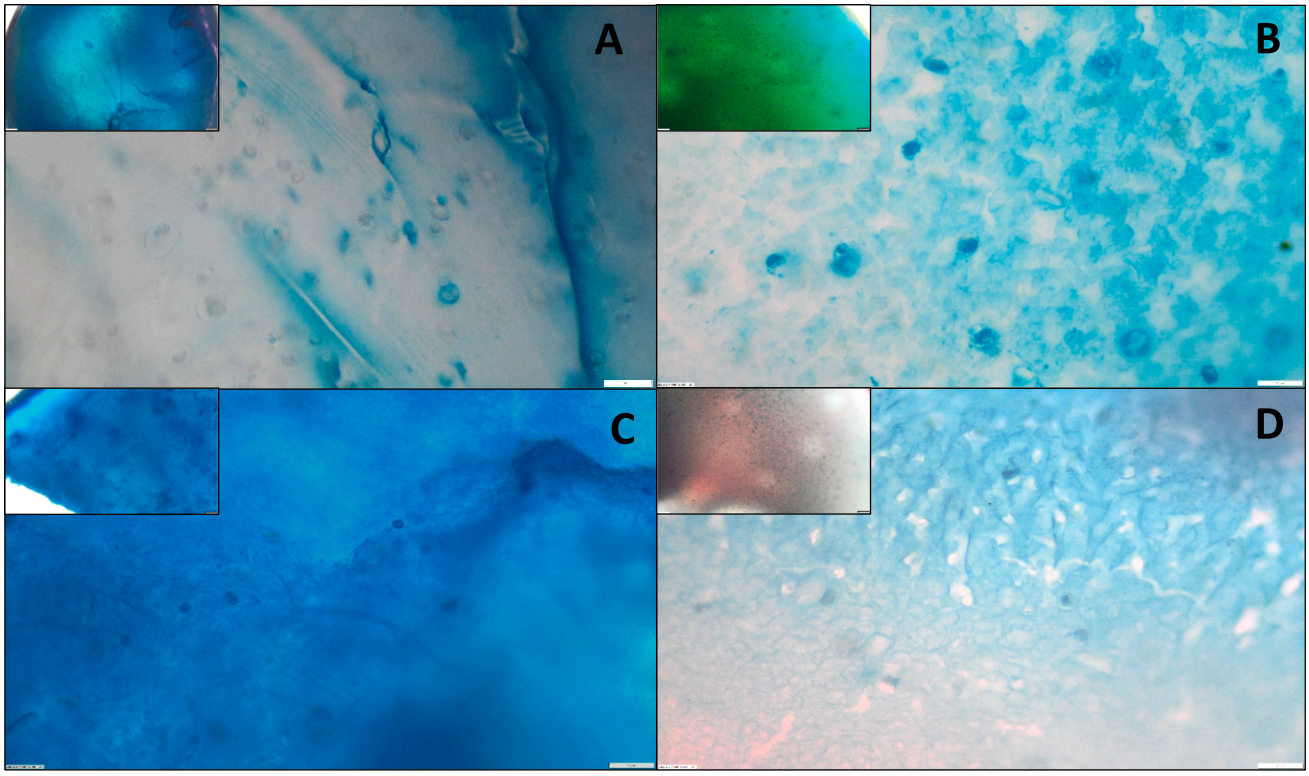

Fig. 8. Histological analysis of hNSCs embedded in NCB (B), NFC (C) or NCC (D) compared to Alginate (A) after 21 days of culture. Images attained from microscopy at 4× (small image) and 20× (large image) magnification are displayed. All materials demonstrate staining with alcian blue with pericellular staining noted most prominently and consistently in B and D, indicating greater ECM deposition. Scale bars (bottom right) depict 50 µm.

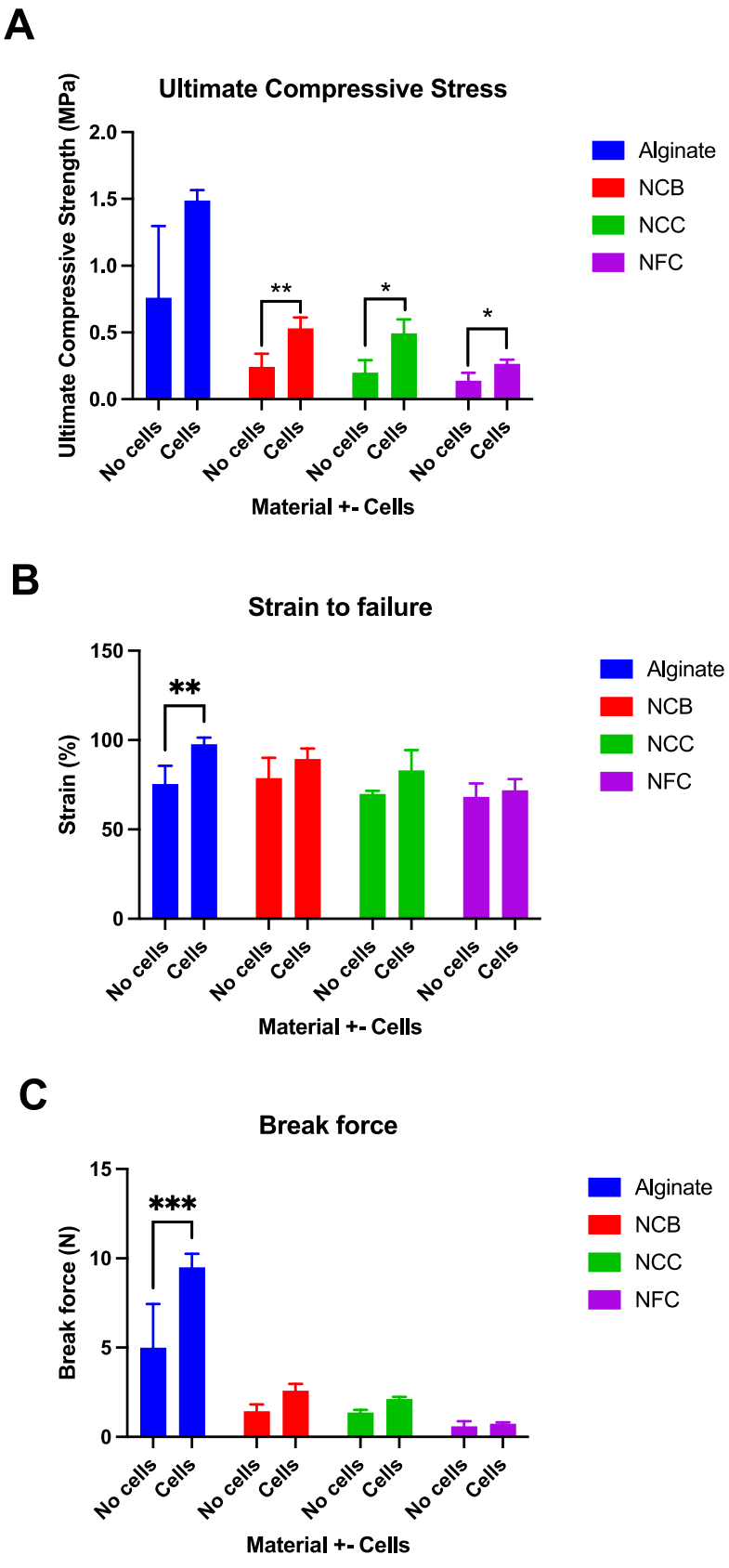

Fig. 10. Mechanical compression testing of materials with and without cells after 21 days of culture. A) The mean UCS of the biomaterials is presented in MPa with error bars depicting standard deviation ($n = 4$). All nanocellulose based materials demonstrated a significant increase in UCS after co-culture with cells. B) The mean strain of the materials (expressed as a percentage) when compressed is presented with and without cells with error bars of standard deviation (n = 4). The strain of alginate was the only material to significantly increase after 21 days of culture with cells. C) The mean break force (Newtons) of each material is presented with standard deviation (n = 4). Increases were observed in all materials after culture with cells but this was only significant for alginate. * = $p < 0.05$; ** = $p < 0.01$; *** = $p < 0.001$.

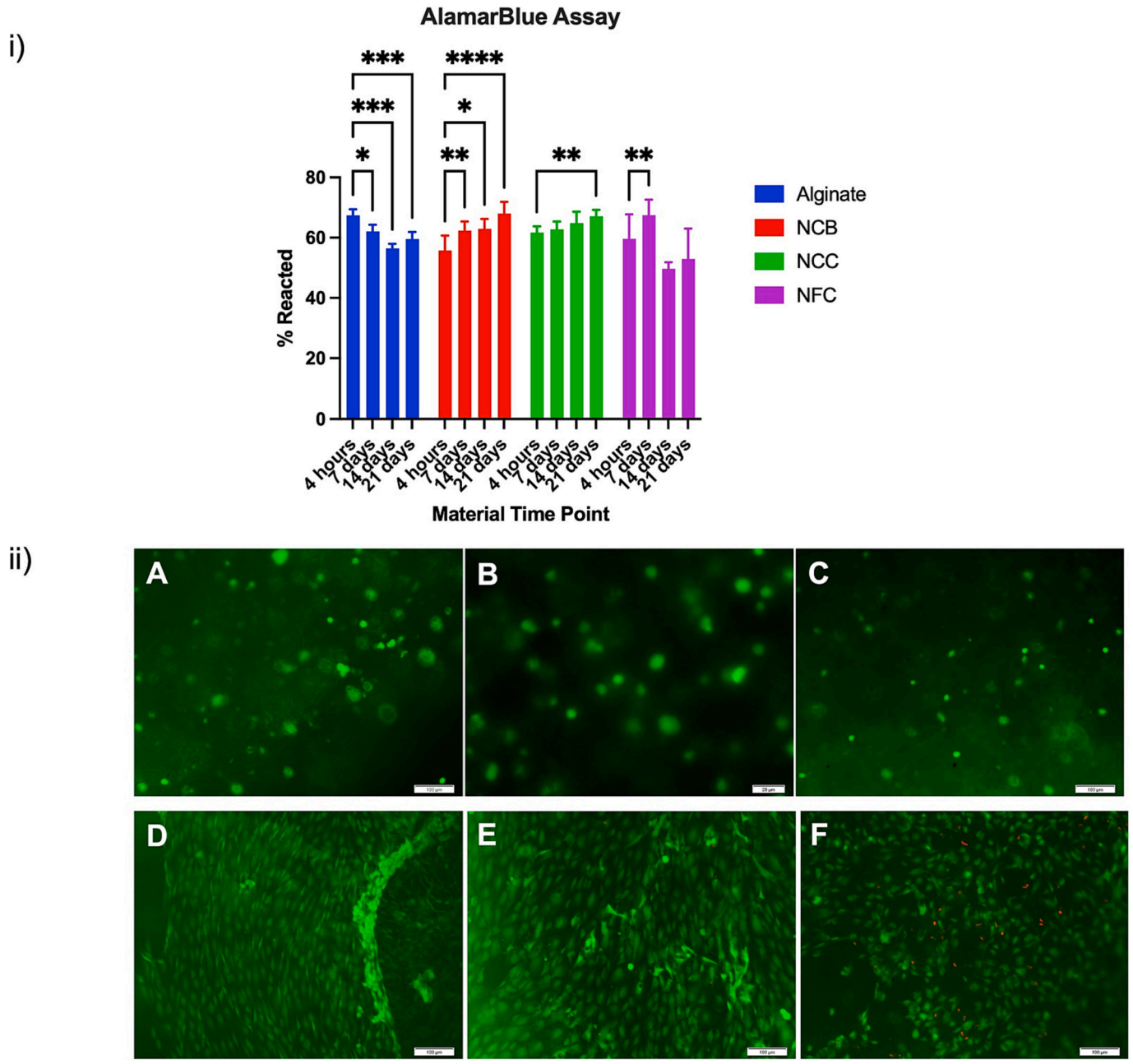

Fig. 11. i) AlamarBlue (AB) Assay demonstrating degree of metabolic activity (as a marker of cell number) in different biomaterials over 21 days. The mean percentage of AB that had been metabolised by cells is expressed relative to negative controls (media and AB only) with error bars depicting standard deviation. Pairwise comparisons were performed using a 2 Way ANOVA and Tukey's multiple comparison test with each material compared to baseline values at 4 h. A total n of 12 is presented (4 repeats from biological triplicates). * = $p < 0.05$; ** = $p < 0.01$; *** = $p < 0.001$, **** = $p < 0.0001$.
ii) Live-dead assay of cell-laden biomaterials at Day 1 (A–C) and Day 21 (D–F). NCB (A, D) demonstrated the highest cell number and viability at 21 days, followed by NCC (B, E) and NFC (C, F). Representative images at 4× magnification, scale bars denote 100 μm.

after culture with cells. The combined findings of high pericellular staining with Alcian blue in the nanocellulose bioinks, and the increase in UCS in nanocellulose bioinks with cells indicates chondrocytes were producing and depositing glycosaminoglycans into the material that contributed to its stiffness.

The degree of strain to failure experienced by the materials was found to generally be higher after culture with cells than without cells (Fig. 10B), but this was only a significant difference in the alginate material ($p = 0.009$). Between materials, the alginate with cells had a significantly higher degree of strain to failure than the NFC (71.9 %, $p = 0.006$) but was not significantly different to the other material with cells. This indicates that despite a higher compressive strength, the alginate with cells became more prone to deformation under compressive loading after culture with cells unlike the nanocellulose based materials.

The break force of the materials expectedly mirrored the UCS (Fig. 10C), showing that the alginate material had the highest break force both without cells (5 MPa) and with cells (9.5 MPa) and that this difference between the two conditions was statistically significant ($p = 0.0001$). The break force with cells was also significantly higher than NCB (1.4 N, $p < 0.0001$), NCC (1.4 N, $p < 0.0001$) and NFC (0.6 N, $p < 0.0001$). There were no significant differences noted between the nanocellulose-based inks with cells, mirroring the ECM assays.

Alginate was considerably stronger in terms of break force and UCS than any of the nanocellulose-alginate composite bioinks. This pertains

to the fact that the nanocellulose used in this study was not crosslinked, and that the strength post-printing is derived from the ionic bonds formed between alginate in the presence of calcium cations. The maximum compressive strength of the nanocellulose-alginate materials with cells was in the region of 0.3–0.6 MPa, which is comparable to previous studies of alginate-hydroxyapatite composite bioinks for bone tissue engineering (0.2–0.9 MPa for 0–40 % hydroxyapatite substitution (Presbítero-Espinosa et al., 2021)) and superior to a bacterial nanocellulose with alginate formulation (in an 80:20 nanocellulose:alginate composition) which had a compressive strength of 33 kPa (Markstedt et al., 2015). Despite these promising mechanical properties, the pulp-derived nanocellulose-alginate materials, remain notably less strong than nasoseptal cartilage which has an UCS of 1.4–3.3 MPa (Al Dayeh & Herring, 2014) and markedly lower than articular cartilage, which has a compressive strength of approximately 36 MPa (Kerin et al., 1998). This emphasises the importance of robust crosslinking to enhance break force and compressive strength, which may be achievable using a cross-linkable formulation such as TEMPO-oxidised nanocellulose (Lin et al., 2012). Augmentation of the durability and mechanical properties of the pulp-derived nanocelluloses will form the basis of future optimisation of these materials for clinical translation.

3.5. Biocompatibility of nanocellulose and alginate bioinks with human chondrocytes

The structure of nanocellulose has been speculated to mirror collagen fibre bundles in ECM, promoting a pro-chondrogenic phenotype (Nguyen et al., 2017). In light of these advantageous structural changes and a closer mimicry of the properties of cartilage ECM, we hypothesised that chondrocytes should favour proliferation in nanocellulose-based inks compared to pure alginate.

NCB and NCC demonstrated an increase in metabolic activity over the course of 21 days: a phenomenon that was not observed in the NFC or alginate materials. Immediately post-bioprinting, all materials demonstrated excellent cell viability with no significant differences noted between material types. Highly significant differences were observed between timepoints ($p < 0.0001$) and materials ($p < 0.0001$) with the alamarBlue assay using a 2-way ANOVA. By 14 and 21 days, the highest mean value of metabolic activity was observed in the NCB (63 % at 14 days, vs Alginate $p = 0.012$, vs NFC $p = 0.0001$; 68 % at 21 days, vs alginate $p < 0.0001$, vs NFC $p = 0.0004$) and NCC materials (64.8 % at 14 days vs Alginate $p = 0.008$, vs NFC $p = 0.0001$; 67.1 % at 21 days vs Alginate $p < 0.0001$, vs NFC $p = 0.0007$), which had both increased significantly from 4 h suggestive of an increase in cell number (NCB 4 h vs 7 days, $p = 0.001$, vs 14 days $p = 0.017$, vs 21 days <0.0001, NCC vs 21 days $p = 0.0024$). There were no significant changes noted between NCB and NCC at any timepoint, indicating a comparably favourable biocompatibility profile and one that was significantly superior to NFC and alginate.

Live dead assays were conducted at 1 and 21 days and demonstrated evidence of chondrocyte proliferation within all nanocellulose biomaterials (Fig. 11). The viability was noted to be greatest in the NCB and lowest in the NFC, which in the latter demonstrated a higher number of dead cells were present. These findings are consistent with the findings observed in the alamarBlue Assay (Fig. 11). Previous studies have explored the chondrogenic potential of bacterially derived nanocellulose fibrils, which owing to their particle width of approximately 100 nm are speculated to be comparable in size to collagen fibrils (Bäckdahl et al., 2006; Fink et al., 1997). Previous scanning and transmission electron microscopy analysis of the nanocellulose formulations used in this study revealed that the nanocellulose crystals demonstrated a length of approximately 100 nm, whereas the fibrillar structures had a mixture of nano and micro surfaces ranging from 100 nm to 100 μm, which lend themselves more favourably to facilitate cell migration and distribution (Kyle et al., 2018; Smith et al., 2009). As such, the NFC, NCC and NCB should all offer biomimicry. On the basis of these experiments, the NCB and NCC appear to be the most conducive bioinks for cell proliferation and viability, which are essential properties for serving the biological needs of cartilage bioprinting.

4. Conclusion

This study highlights the promise of nanocellulose-based bioinks for 3D bioprinting facial cartilage. In this study, the hypothesis was that the inclusion of nanocellulose into an alginate bioink would enhance the biological and mechanical properties of the bioink for 3D bioprinting cartilage and demonstrate improvements in printability, biocompatibility and chondrogenicity. Furthermore, it was hypothesised that based on our previous structural characterisation of NCB, NCC and NFC that the structural subtypes of nanocellulose would translate to differences in chondrocyte behaviour and printability. This study offers a novel insight into the biological benefits of different nanocellulose structural subtypes for cartilage tissue engineering in direct comparison with alginate. Specifically, this study identified that all nanocellulose-alginate bioinks display superiority in printability, demonstrating the fidelity and resolution necessary to produce recognisable complex anatomical structures such as an auricular antihelix. Moreover, biologically, pulp-derived nanocelluloses demonstrated a pro-chondrogenic environment, with sustained elevations in chondrogenic gene expression that surpassed alginate, and evidence of subsequent pericellular matrix deposition that translates to increased compressive strength of the material. The novelty of this study lies in the translationally-focussed comparison of nanocellulose structural subtypes with alginate, offering a biological insight into the most suitable biomaterials for bioink development. Whilst there are subtle differences between the nanocellulose subtypes in terms of printability and biological behaviours, all pulp-derived nanocelluloses have demonstrated tremendous promise for 3D bioprinting cartilage tissue for clinical use. In particular, NCB and NCC variants appear to offer superior biocompatibility, with NCC holding the most promise for the biofabrication of auricular or nasoseptal cartilage tissue replacements owing to its unparalleled chondrogenic potential. The limitations of the nanocelluloses used in this study pertain to their lack of crosslinking activity relative to pure alginate, which currently limits their mechanical strength. As such, future efforts to enhance crosslinking of pulp-derived nanocelluloses are warranted prior to progressing towards clinical translation and in vivo studies.

CRediT authorship contribution statement

Thomas H. Jovic: Conceptualization, Data curation, Formal analysis, Funding acquisition, Investigation, Methodology, Project administration, Resources, Visualization, Writing – original draft. **Tamsin Nicholson:** Methodology, Formal analysis, Investigation. **Hari Arora:** Conceptualization, Methodology, Resources, Investigation, Data curation. **Kim Nelson:** Formal analysis, Methodology, Resources, Writing - review & editing. **Shareen H. Doak:** Conceptualization, Methodology, Resources, Writing – review & editing, Supervision, Project administration. **Iain S. Whitaker:** Conceptualization, Methodology, Resources, Writing – review & editing, Supervision, Project administration, Funding acquisition.

Declaration of competing interest

The authors declare the following financial interests/personal relationships which may be considered as potential competing interests:

Iain Whitaker, Kim Nelson has patent #US16/976,803 pending to AVAPCO.

Data availability

Data will be made available on request.

Acknowledgements

The authors would like to acknowledge the support of AVAPCO for supplying the nanocelluloses and Ms. Kavitha Saw for supplying the nasoseptal cartilage samples for chondrocytes used in this study.

This study was supported by The Scar Free Foundation & Health and Care Research Wales Programme of research in Reconstructive Surgery & Regenerative Medicine, which has been established in the ReconRegen Research Centre at Swansea University in partnership with Swansea Bay University Health Board.

This work was additionally supported by Action Medical Research and the VTCT Foundation (Grant Number 2782), the Royal College of Surgeons England and the Welsh Clinical Academic Training Programme.

Appendix A. Supplementary data

Supplementary data to this article can be found online at https://doi.org/10.1016/j.carbpol.2023.121261.

References

Aarstad, O., Heggset, E. B., Pedersen, I. S., Bjørnøy, S. H., Syverud, K., & Strand, B. L. (2017). Mechanical properties of composite hydrogels of alginate and cellulose nanofibrils. *Polymers, 9*(8). https://doi.org/10.3390/polym9080378

Al Dayeh, A. A., & Herring, S. W. (2014). Compressive and tensile mechanical properties of the porcine nasal septum. *Journal of Biomechanics, 47*(1), 154. https://doi.org/10.1016/J.JBIOMECH.2013.09.026

Al-Sabah, A., Burnell, S. E. A., Simoes, I. N., Jessop, Z., Badiei, N., Blain, E., & Whitaker, I. S. (2019). Structural and mechanical characterization of crosslinked and sterilised nanocellulose-based hydrogels for cartilage tissue engineering. *Carbohydrate Polymers, 212*, 242–251. https://doi.org/10.1016/j.carbpol.2019.02.057

Athanasiou, K. A., Niederauer, G. G., & Agrawal, C. M. (1996). Sterilization, toxicity, biocompatibility and clinical applications of polylactic acid/ polyglycolic acid copolymers. *Biomaterials, 17*(2), 93–102. https://doi.org/10.1016/0142-9612(96)85754-1

Axpe, E., & Oyen, M. L. (2016). Applications of alginate-based bioinks in 3D bioprinting. *International Journal of Molecular Sciences, 17*(12). https://doi.org/10.3390/ijms17121976

Bäckdahl, H., Helenius, G., Bodin, A., Nannmark, U., Johansson, B. R., Risberg, B., & Gatenholm, P. (2006). Mechanical properties of bacterial cellulose and interactions with smooth muscle cells. *Biomaterials, 27*(9), 2141–2149. https://doi.org/10.1016/J.BIOMATERIALS.2005.10.026

Chimene, D., Lennox, K. K., Kaunas, R. R., & Gaharwar, A. K. (2016). Advanced bioinks for 3D printing: A materials science perspective. *Annals of Biomedical Engineering, 44*(6), 2090–2102. https://doi.org/10.1007/s10439-016-1638-y

Dashtdar, H., Murali, M. R., Selvaratnam, L., Raghavendran, H. B., Suhaeb, A. M., Ahmad, T. S., & Kamarul, T. (2016). Ultra-structural changes and expression of chondrogenic and hypertrophic genes during chondrogenic differentiation of mesenchymal stromal cells in alginate beads. *PeerJ, 2016*(3). https://doi.org/10.7717/PEERJ.1650/SUPP-1

Dunlop, M. J., Clemons, C., Reiner, R., Sabo, R., Agarwal, U. P., Bissessur, R., … Acharya, B. (2020). Towards the scalable isolation of cellulose nanocrystals from tunicates. *Scientific Reports 2020 10:1, 10*(1), 1–13. https://doi.org/10.1038/s41598-020-76144-9

Ewa-Choy, Y. W., Pingguan-Murphy, B., Abdul-Ghani, N. A., Jahendran, J., & Chua, K. H. (2017). Effect of alginate concentration on chondrogenesis of co-cultured human adipose-derived stem cells and nasal chondrocytes: A biological study. *Biomaterials Research, 21*(1). https://doi.org/10.1186/S40824-017-0105-7

Fink, H. P., Purz, H. J., Bohn, A., & Kunze, J. (1997). Investigation of the supramolecular structure of never dried bacterial cellulose. *Macromolecular Symposia, 120*(1), 207–217. https://doi.org/10.1002/MASY.19971200121

Freeman, F. E., & Kelly, D. J. (2017). Tuning alginate bioink stiffness and composition for controlled growth factor delivery and to spatially direct MSC fate within bioprinted tissues. *Scientific Reports 2017 7:1, 7*(1), 1–12. https://doi.org/10.1038/s41598-017-17286-1

Gershlak, J. R., Hernandez, S., Fontana, G., Perreault, L. R., Hansen, K. J., Larson, S. A., … Gaudette, G. R. (2017). Crossing kingdoms: Using decellularized plants as perfusable tissue engineering scaffolds. *Biomaterials, 125*, 13–22. https://doi.org/10.1016/J.BIOMATERIALS.2017.02.011

Han, L., Grodzinsky, A. J., & Ortiz, C. (2011). Nanomechanics of the cartilage extracellular matrix. *Annual Review of Materials Research, 41*, 133. https://doi.org/10.1146/ANNUREV-MATSCI-062910-100431

Hazur, J., Detsch, R., Karakaya, E., Kaschta, J., Teßmar, J., Schneidereit, D., … Boccaccini, A. R. (2020). Improving alginate printability for biofabrication: Establishment of a universal and homogeneous pre-crosslinking technique. *Biofabrication, 12*(4), Article 045004. https://doi.org/10.1088/1758-5090/AB98E5

Jessop, Z. M., Al-Sabah, A., Gao, N., Kyle, S., Thomas, B., Badiei, N., … Whitaker, I. S. (2019). Printability of pulp derived crystal, fibril and blend nanocellulose-alginate bioinks for extrusion 3D bioprinting. *Biofabrication, 11*(4), Article 045006. https://doi.org/10.1088/1758-5090/ab0631

Jessop, Z. M., Al-Sabah, A., Gardiner, M. D., Combellack, E., Hawkins, K., & Whitaker, I. S. (2017). 3D bioprinting for reconstructive surgery: Principles, applications and challenges. *Journal of Plastic, Reconstructive & Aesthetic Surgery, 70*(9), 1155–1170. https://doi.org/10.1016/j.bjps.2017.06.001

Jovic, T. H., Kungwengwe, G., Mills, A. C., & Whitaker, I. S. (2019). Plant-derived biomaterials: A review of 3D bioprinting and biomedical applications. In , *Vol. 5*. *Frontiers in mechanical engineering*. https://doi.org/10.3389/fmech.2019.00019. Frontiers Media SA.

Kerin, A. J., Wisnom, M. R., & Adams, M. A. (1998). The compressive strength of articular cartilage. *Proceedings of the Institution of Mechanical Engineers. Part H, Journal of Engineering in Medicine, 212*(4), 273–280. https://doi.org/10.1243/0954411981534051

Kyle, S., Jessop, Z. M., Al-Sabah, A., Hawkins, K., Lewis, A., Maffeis, T., … Whitaker, I. S. (2018). Characterization of pulp derived nanocellulose hydrogels using AVAP® technology. *Carbohydrate Polymers, 198*, 270–280. http://www.ncbi.nlm.nih.gov/pubmed/30093000.

Kyle, S., Jessop, Z. M., Al-Sabah, A., & Whitaker, I. S. (2017). Printability of candidate biomaterials for extrusion based 3D printing: State-of-the-art. *Advanced Healthcare Materials, 6*(16), 1700264. https://doi.org/10.1002/adhm.201700264

Lee, K. Y., & Mooney, D. J. (2012). Alginate: Properties and biomedical applications. *Progress in Polymer Science, 37*(1), 106–126. https://doi.org/10.1016/j.progpolymsci.2011.06.003

Lefebvre, V., Angelozzi, M., & Haseeb, A. (2019). SOX9 in cartilage development and disease. *Current Opinion in Cell Biology, 61*, 39–47. https://doi.org/10.1016/J.CEB.2019.07.008

Lin, N., Bruzzese, C., & Dufresne, A. (2012). TEMPO-oxidized nanocellulose participating as crosslinking aid for alginate-based sponges. *ACS Applied Materials and Interfaces, 4*(9), 4948–4959. https://doi.org/10.1021/AM301325R

Lin, N., & Dufresne, A. (2014). Nanocellulose in biomedicine: Current status and future prospect. *European Polymer Journal, 59*, 302–325. https://doi.org/10.1016/J.EURPOLYMJ.2014.07.025

Livak, K. J., & Schmittgen, T. D. (2001). Analysis of relative gene expression data using real-time quantitative PCR and the 2-ΔΔCT method. *Methods, 25*(4), 402–408. https://doi.org/10.1006/meth.2001.1262

Ma, T., Lv, L., Ouyang, C., Hu, X., Liao, X., Song, Y., & Hu, X. (2021). Rheological behavior and particle alignment of cellulose nanocrystal and its composite hydrogels during 3D printing. *Carbohydrate Polymers, 253*, Article 117217. https://doi.org/10.1016/J.CARBPOL.2020.117217

Malda, J., Visser, J., Melchels, F. P., Jüngst, T., Hennink, W. E., Dhert, W. J. A., … Hutmacher, D. W. (2013). 25th anniversary article: Engineering hydrogels for biofabrication. *Advanced Materials, 25*(36), 5011–5028. https://doi.org/10.1002/adma.201302042

Markstedt, K., Mantas, A., Tournier, I., Martínez Ávila, H., Hägg, D., & Gatenholm, P. (2015). 3D bioprinting human chondrocytes with nanocellulose-alginate bioink for cartilage tissue engineering applications. *Biomacromolecules, 16*(5), 1489–1496. https://doi.org/10.1021/acs.biomac.5b00188

Martínez Ávila, H., Feldmann, E. M., Pleumeekers, M. M., Nimeskern, L., Kuo, W., de Jong, W. C., … Gatenholm, P. (2015). Novel bilayer bacterial nanocellulose scaffold supports neocartilage formation in vitro and in vivo. *Biomaterials, 44*, 122–133. https://doi.org/10.1016/J.BIOMATERIALS.2014.12.025

Martínez Ávila, H., Schwarz, S., Rotter, N., & Gatenholm, P. (2016). 3D bioprinting of human chondrocyte-laden nanocellulose hydrogels for patient-specific auricular cartilage regeneration. *Bioprinting, 1–2*, 22–35. https://doi.org/10.1016/J.BPRINT.2016.08.003

Möller, T., Amoroso, M., Hägg, D., Brantsing, C., Rotter, N., Apelgren, P., … Gatenholm, P. (2017). In vivo Chondrogenesis in 3D bioprinted human cell-laden hydrogel constructs. *Plastic and Reconstructive Surgery - Global Open, 5*(2), Article e1227. https://doi.org/10.1097/GOX.0000000000001227

Müller, M., Öztürk, E., Arlov, Ø., Gatenholm, P., & Zenobi-Wong, M. (2017). Alginate sulfate–Nanocellulose bioinks for cartilage bioprinting applications. *Annals of Biomedical Engineering, 45*(1), 210–223. https://doi.org/10.1007/s10439-016-1704-5

Nelson, K., & Restina, T. (2014). Innovative nanocellulose process breaks the cost barrier. *Tappi Journal, 13*(5), 19–23. https://doi.org/10.32964/TJ13.5.19

Nguyen, D., Hgg, D. A., Forsman, A., Ekholm, J., Nimkingratana, P., Brantsing, C., … Simonsson, S. (2017). Cartilage tissue engineering by the 3D bioprinting of iPS cells in a nanocellulose/alginate bioink. *Scientific Reports 2017 7:1, 7*(1), 1–10. https://doi.org/10.1038/s41598-017-00690-y

O'Brien, F. J. (2011). Biomaterials & scaffolds for tissue engineering. *Materials Today, 14*(3), 88–95. https://doi.org/10.1016/S1369-7021(11)70058-X

Pääkko, M., Ankerfors, M., Kosonen, H., Nykänen, A., Ahola, S., Österberg, M., … Lindström, T. (2007). Enzymatic hydrolysis combined with mechanical shearing and high-pressure homogenization for nanoscale cellulose fibrils and strong gels. *Biomacromolecules, 8*(6), 1934–1941. https://doi.org/10.1021/bm061215p

Park, S. Y., Kim, W.-J., Choi, J. B., & Kim, S. (2018). Physical and mechanical properties of alginate-based hydrogel film as carrier for release of acetylthiocholine. *International Journal of Precision Engineering and Manufacturing, 19*(1), 129. https://doi.org/10.1007/s12541-018-0015-1

Piras, C. C., & Smith, D. K. (2020). Multicomponent polysaccharide alginate-based bioinks. *Journal of Materials Chemistry B, 8*(36), 8171–8188. Royal Society of Chemistry https://doi.org/10.1039/d0tb01005g.

Presbítero-Espinosa, G., Peña-Parás, L., Sánchez-Fernández, J. A., Pizaña, E. I. R., Galván, K. P. V., Vopálenský, M., … Elizalde-Herrera, L. E. (2021). Characterization of sodium alginate hydrogels reinforced with nanoparticles of hydroxyapatite for biomedical applications. *Polymers, 13*(17), 2927. https://doi.org/10.3390/POLYM13172927

Sarkar, K., Xue, Y., & Sant, S. (2017). Host response to synthetic versus natural biomaterials. In *The immune response to implanted materials and devices* (pp. 81–105). Springer International Publishing. https://doi.org/10.1007/978-3-319-45433-7_5.

Siqueira, P., Siqueira, É., Lima, A. E.d., Siqueira, G., Pinzón-Garcia, A. D., Lopes, A. P., … Botaro, V. R. (2019). Three-dimensional stable alginate-nanocellulose gels for biomedical applications: Towards tunable mechanical properties and cell growing. *Nanomaterials, 9*(1). https://doi.org/10.3390/NANO9010078

Smith, I. O., Liu, X. H., Smith, L. A., & Ma, P. X. (2009). Nanostructured polymer scaffolds for tissue engineering and regenerative medicine. *Wiley Interdisciplinary Reviews: Nanomedicine and Nanobiotechnology, 1*(2), 226–236. https://doi.org/10.1002/WNAN.26

Tarassoli, S. P., Jessop, Z. M., Jovic, T., Hawkins, K., & Whitaker, I. S. (2021). Candidate bioinks for extrusion 3D bioprinting—A systematic review of the literature. *Frontiers in Bioengineering and Biotechnology, 0*, 383. https://doi.org/10.3389/FBIOE.2021.616753

Taylor, M. S., Daniels, A. U., Andriano, K. P., & Heller, J. (1994). Six bioabsorbable polymers: In vitro acute toxicity of accumulated degradation products. *Journal of Applied Biomaterials, 5*(2), 151–157. https://doi.org/10.1002/jab.770050208

Tibbitt, M. W., & Anseth, K. S. (2009). Hydrogels as extracellular matrix mimics for 3D cell culture. *Biotechnology and Bioengineering, 103*(4), 655–663. https://doi.org/10.1002/BIT.22361

Torres, F. G., Commeaux, S., & Troncoso, O. P. (2012). Biocompatibility of bacterial cellulose based biomaterials. *Journal of Functional Biomaterials, 3*(4), 864–878. https://doi.org/10.3390/JFB3040864

Wee, & Gombotz. (1998). Protein release from alginate matrices. *Advanced Drug Delivery Reviews, 31*(3), 267–285. http://www.ncbi.nlm.nih.gov/pubmed/10837629.

Yang, I. H., Kim, S. H., Kim, Y. H., Sun, H. J., Kim, S. J., & Lee, J. W. (2004). Comparison of phenotypic characterization between “alginate bead” and “pellet” culture systems as chondrogenic differentiation models for human mesenchymal stem cells. *Yonsei Medical Journal, 45*(5), 891–900. https://doi.org/10.3349/YMJ.2004.45.5.891

Yegappan, R., Selvaprithiviraj, V., Amirthalingam, S., & Jayakumar, R. (2018). Carrageenan based hydrogels for drug delivery, tissue engineering and wound healing. *Carbohydrate Polymers, 198*, 385–400. https://doi.org/10.1016/J.CARBPOL.2018.06.086